Journal of Hazardous Materials 472 (2024) 134528

Contents lists available at ScienceDirect

Journal of Hazardous Materials

journal homepage: www.elsevier.com/locate/jhazmat

Sea–level rise and arsenic–rich soils: A toxic relationship

Fatemeh Izaditame [a,*], Joshua J. LeMonte [c], Matthew G. Siebecker [d], Xuan Yu [e], Matthew Fischel [f], Ryan Tappero [g], Donald L. Sparks [b]

[a] Department of Sustainable Earth Systems Sciences, University of Texas at Dallas, Richardson, TX 75080, USA
[b] Department of Plant & Soil Sciences, University of Delaware, Newark, DE 19716, USA
[c] Department of Geological Sciences, Brigham Young University, Provo, UT 84602, USA
[d] Department of Plant and Soil Science, Texas Tech University, Lubbock, TX 79409, USA
[e] State Key Laboratory of Soil and Sustainable Agriculture, Institute of Soil Science, Chinese Academy of Sciences, Nanjing 210008, China
[f] Sustainable Agricultural Systems Laboratory, USDA–Agricultural Research Service, Beltsville, MD 20705, USA
[g] Soil Scientist, Brookhaven National Laboratory, Upton, NY 11973, USA

HIGHLIGHTS

- Studied As–contaminated soils response to SLR through hydrogeochemical analysis.
- Contaminated urban soils contained up to 6% As hotspots.
- Natural seawater and river water inundation increases As release.
- Observed As release as high as ca. 200 times more than EPA threshold.
- Sea–level rise can significantly contribute to As release.

GRAPHICAL ABSTRACT

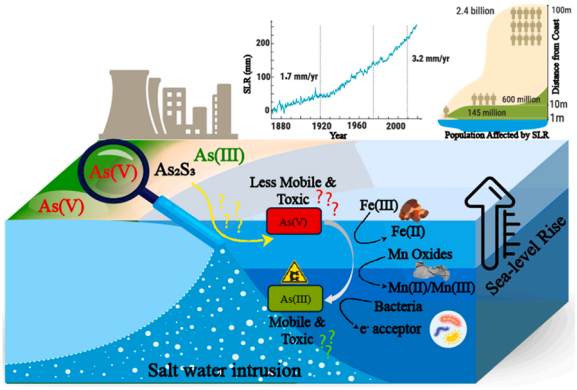

ARTICLE INFO

Keywords:
X-ray absorption spectroscopy
Sea-level rise
Coastal Soils
Arsenic
Speciation
Water pollution

ABSTRACT

In the United States, dangerously high arsenic (As) levels have been found in drinking water wells in more than 25 states, potentially exposing 2.1 million people to drinking water high in As; a known carcinogen. The anticipated sea–level rise (SLR) is expected to alter soil biogeochemical and hydrological conditions, potentially impacting their ability to sequester As. In our study of coastal Wilmington, DE, an area projected to experience a 1 –meter SLR by 2100, we examined the spatial distribution, speciation, and release possibilities of As due to SLR. To understand the complex dynamics at play, we employed a comprehensive approach, including bulk and micro X–ray absorption spectroscopy measurements, hydrological pattern evaluation, and macroscopic stirred–flow experiments. Our results suggest that introducing reducing and saline conditions can increase As release in both river water and seawater inundation scenarios, most likely due to ionic competition and the dissolution of As–bearing Fe/Mn oxides. Regardless of the salinity source, the released As concentrations

* Corresponding author.
E-mail addresses: izadi@utdallas.edu (F. Izaditame), lemonte@byu.edu (J.J. LeMonte), Matthew.Siebecker@ttu.edu (M.G. Siebecker), yuxuan@issas.ac.cn (X. Yu), Matthew.Fischel@usda.gov (M. Fischel), rtappero@bnl.gov (R. Tappero), dlsparks@udel.edu (D.L. Sparks).

https://doi.org/10.1016/j.jhazmat.2024.134528
Received 5 March 2024; Received in revised form 25 April 2024; Accepted 1 May 2024
Available online 3 May 2024
0304-3894/© 2024 Elsevier B.V. All rights reserved.

consistently exceeded the EPA threshold for drinking water. Our results provide valuable insights for developing appropriate remedial and management strategies for this site and numerous others facing similar environmental challenges.

Environmental Implication: With nearly two hundred million individuals living within coastal flood plains and with two million square kilometers of land and one trillion dollars' worth of assets lying less than 1 m above current sea level, sea–level rise (SLR) is one of the significant socio–economic threats associated with global warming. Arsenic is a prevalent contaminant in coastal areas impacted by industrial activities, many of which are susceptible to being impacted by SLR. This study examines SLR's impact on arsenic fate and speciation in a densely populated coastline in Wilmington, DE, expecting 1 meter of SLR by 2100.

1. Introduction

Urban coastal areas often have a history of contamination due to previous land use and reclamation practices, including using arsenic (As) in industrial and agricultural processes. This issue is particularly pronounced in countries such as Argentina, Bangladesh, Cambodia, Chile, China, India, Mexico, Pakistan, the United States, and Vietnam, where elevated levels of inorganic As contaminate water resources [3]. Climate-induced Sea−level rise (SLR) and the expected increased extreme weather events [82,83] can exacerbate the quality of soil and water resources that are contaminated with As by altering soil redox conditions and salinity, which can lead to the release of this toxic element. This can be a significant problem in contaminated coastal areas where existing remediation efforts do not always account for SLR and the risk of SLR−associated flooding.

Arsenic is a hazardous, redox−sensitive element and a contaminant of significant concern in global environmental regulations [12]. Exposure to As can happen in solution (water) and solid (soils and sediments) phases, leading to health risks such as skin, lung, bladder, and other internal organ cancers [44]. In the environment, As exists primarily in two oxidation states –arsenite [As(III)] (dominant in anaerobic environments) and arsenate [As(V)] (dominant under well–aerated conditions) [19,2,61,75]. Among other species, As(III) exhibits the highest mobility and toxicity in solids as the neutral species (H_3AsO_3) [4].

Arsenic contamination of urban soils is widely reported (e.g., [31,41, 27,39]), with some solid phase As concentrations reaching as high as 60, 000 mg kg^{-1} [33]. In the United States, As contaminates more than a third of all National Priority List (Superfund) Sites, the most contaminated hazardous waste sites in the US, and nearly half of public groundwater supplies ([21,72]). Nearly 60% of the US Superfund sites will be directly affected by natural hazards exacerbated by climate change such as flooding and SLR [29]. Arsenic is also a prevalent contaminant in coastal areas impacted by industrial activities [39], many of which are susceptible to being impacted by SLR. However, there is limited understanding of the effects of climate−change−induced perturbations, including SLR, on the mobilization of As and other contaminants from contaminated coastal sites.

The environmental risks associated with As are contingent on As concentration and solid−phase speciation, as the latter plays a crucial role in determining both As mobility and toxicity [21,63]. Although studies of As distribution and speciation in As−rich soils have been conducted (e.g., [41,86,26,17,69,38]), spatially resolved information on As distribution and speciation in soils subject to SLR and their response to SLR−associated stressors is currently not available but may provide new insights into planning for the expected scenarios. A robust understanding of As characterization is essential to developing accurate risk assessment models and formulating reliable remediation strategies for the sites that SLR may influence.

To understand the long−term behavior of As in complex dynamic systems, such as contaminated urban coastal environments, a synergistic approach is required to incorporate chemical analysis and spectroscopic techniques. While bulk As K−edge XAS analyses offer insights into the average coordination environment of As, they fall short in providing information on its spatial distribution, elemental correlations, and chemical speciation at the microscale and may also fail to detect minor As species with potential high geochemical activity. In this study, therefore, bulk and micro−scale spectroscopic analysis are combined with chemical measurements and hydrological analysis to thoroughly investigate two highly As−contaminated sites (including a Superfund site), a tidally influenced remedial drainage ditch, and the Christina riverbank soils at the city of Wilmington, in New Castle County, Delaware. In recent years, elevated As levels were detected in the ditch and groundwater [33,39,84], indicating contaminant migration from adjacent industrial sites to the ditch. This region, prone to periodic flooding from the Christina River and urban runoff, is projected to face inundation by 1 m of SLR by 2100. Due to the hydrologic conditions and the geochemical zonation, we anticipate that the As concentration in the area will continue to increase, resulting in As accumulation in the ditch. Over ten years (2005−2014), the average As content in the ditch soils increased from 390 to 13,300 mg kg^{-1} [84] and from 13,300 to 33,200 mg kg^{-1} from 2014 to 2019. The anticipated increase in As concentration, combined with the expected changes in hydrology such as the increase in sea levels, enhances the risk of As release from these contaminated coastal soils.

This study provides the first information on the multiscale (micro- and bulk- scale) distribution and speciation of As in a redox−dynamic flood−prone contaminated coastal environment and evaluates its response to the current and expected hydrological patterns. Specifically, the objectives include evaluating changes in As concentration and speciation in soil profiles to assess the risk of surface water and groundwater contamination, identifying the As source in the drainage ditch, discerning differences in As chemistry at micro and bulk scales, and assessing the impacts of current hydrological patterns and future SLR scenarios on As release. Our results provide a solid evidence base for assessing the long−term risk of As to human health and ecosystems in dynamic urban environments facing SLR.

2. Material and methods

2.1. Study Site

The study site is on the Delmarva Peninsula along the Atlantic coastal plain of the eastern seaboard of Delaware, U.S.A (Fig. S1). Characterized by a continental climate, the region experiences an average rainfall of 109 cm and average temperature of 12°C [20]. The sampled area, with a history of contamination, encompasses four distinct sections: (1) a former chemical production plant listed on the Superfund National Priority List by the U.S. Environmental Protection Agency (EPA) due to contamination from As trioxide use as a raw ingredient in its production processes (hereafter Site H); (2) a former ore processing factory now regulated under the state of Delaware's Hazardous Substance and Control Act, marked by contamination resulting from several decades of As−bearing pyrite ore roasting activities (hereafter Site P); (3) The bank and base of a tidally−influenced ditch constructed as part of a remediation effort for the neighboring Sites H and P; and (4) the south bank of the tidal Christina River in South Wilmington, DE. Site H and Site P will also be collectively called the "Sites" in this paper. The soils of the sampled area include fine−silty, mixed, active, mesic Typic Endoaquults

(Site H); Udorthents and urban land (Site P); and Udorthents (the Christina Riverbank and the bank and base of the constructed ditch). The underlying bedrock in the area is characterized by the Lower Cretaceous Period Potomac formation, featuring variegated silts and clays with beds of quartz sand. Due to litigation regarding the cleanup of these sites, precise locations are withheld.

In recent years, elevated As levels were detected in the remedial ditch (up to 60,000 mg kg^{-1}) and groundwater [33,39,84], indicating contaminant migration from the industrial sites to the ditch. The ditch feeds directly into the Christina River, is approximately 150 m x 10 m with its base about 1 m below sea level, and its bank reaching 5 m above sea level (see Fig. S2). The ditch and riverbank soils experience episodes of wetting/drying as the site periodically floods from the Christina River and urban runoff and is influenced by tides [84]. Extreme weather often impacts the area, including nor−easters, coastal flooding, heavy rainfall, and severe thunderstorms. Portions of the study area are also projected to be inundated by 1 m of SLR by 2100 (Fig. 6; [18]). The added influence of SLR and tides makes this site susceptible to shifting hydrologic and redox regimes on daily, monthly, and seasonal scales that can affect As redox state and subsequent mobility and toxicity in surface− and ground−water resources.

2.2. Sample collection and characterization

To gain a general understanding of the chemical composition and oxidation state of As, the first group of samples was collected as single cores using a Geoprobe direct push drill from Site H, Site P, and the ditch bank. These cores were extracted and logged from the ground down to 3.7 m below the surface. To avoid enhanced release of As from the ditch base, a direct push hand corer was used to collect a core to the depth of the refusal (0.2 m) due to engineered riprap. Upon recovery, the cores were promptly capped, wrapped in polyethylene film to prevent oxidation, and transported on ice to an anaerobic chamber for storage and processing within a 6−hour timeframe. Subsamples were carefully selected from each core based on observable changes in the soil profile, such as alterations in color or texture, typically occurring every 15-30 cm. These subsamples were subsequently dried in an anaerobic chamber, lightly ground to pass through a 2 mm sieve, and stored in the dark at 4°C until bulk geochemical analysis was conducted (Table 1). The total free iron oxide content of the cores from the ditch base, Site H, and Site P was determined using the citrate−bicarbonate−dithionite method [40]. Additionally, As bound by inner/outer−sphere complexation and/or occlusion has been previously assessed by [39] through sequential extraction following the methodology outlined by [77].

To conduct a more detailed study of As concentration and distribution in areas near the river, where SLR and tidal impacts are more pronounced and the contamination issue is escalating, surface soil samples 0-0.3 m) were systematically collected at sixteen locations using shovel. These locations were randomly chosen from both downstream (closer to the river, labeled D1−D6) and upstream (farther away from the river, labeled D7−D10) sections of the ditch, as well as the Christina riverbank (labeled R1−R6) (refer to Fig. S1 and Fig. 2, Panel a). At each location, soil samples were collected at 0 — 30 cm and stored separately in sealed plastic bags inside plastic containers, passed through a 4 mm sieve at field moisture, and remained in a cold room (4°C) during the entire time prior to experiments to prevent possible change in oxidation state. A ca. 200 g subsample of each soil sample was air−dried under a fume hood and analyzed for pH (1:1 water), organic matter (OM, loss on ignition), and particle size distribution (hydrometer method) following [65] (Table S.1). Total As and other select element concentrations (Al, Cr, Fe, Pb, S, and Mn) of the homogenized samples were determined by microwave–acid digestion [1,71], followed by analysis via inductively coupled plasma atomic emission spectrometry (ICP–AES, Thermo Elemental Intrepid II XSP Duo View) (Table 2).

2.3. X−ray Absorption Spectroscopy (XAS)

2.3.1. Bulk XAS

Separate cores from Site H, Site P, and the ditch bank and base were subsampled in 120 cm increments for the bulk synchrotron−based analysis. The cores were subsampled with N_2 passing over each core into vials that were then flushed with N_2 and immediately placed into an anaerobic glove bag to preserve the oxidation state. Once in the glove bag, samples were air dried under an anaerobic (95% N_2/5% H_2) atmosphere, homogenized to a fine powder, and stored in the inert atmosphere until synchrotron analyses. Arsenic K−edge X–ray absorption near–edge structure (XANES) was collected at the Brazilian Synchrotron Light Laboratory (LNLS) and the Canadian Light Source (CLS). For more details, see Text S1. For samples D1–D10 and R1–R6, As K–edge XANES spectroscopy was performed at the XFM beamline (4−BM) of the National Synchrotron Light Source II (NSLS–II), Brookhaven National Laboratory (Upton, NY, USA). For more information, see Text S2.

2.3.2. Microfocused X−ray analysis

The bulk As K–edge XANES spectra represent a weighted average of As forms within a sample. Therefore, only the dominant As species will be represented using linear combination fitting (LCF), and the minor species will not significantly contribute to the spectra in the bulk analysis. To understand the spatial heterogeneity of As valence states and to determine elemental hot spots, colocation patterns, and mineralogy, fine–scale μ−XRF mapping, μ–XANES spectroscopy, and micro−X−ray diffraction (μ−XRD) patterns were acquired at the XFM beamline (4–BM) at NSLS–II for the ditch (D2 and D7) and riverbank soils (R3 and R4) and the oxidation states of As at several hot spots were measured. The air−dried samples representative of the upstream (D2) and downstream (D7) of the tidal ditch and the riverbank (R3 and R4) were

Table 1
The elemental composition of soil samples collected from the ditch base, ditch bank, and Sites H and P. Characteristics of Site H at 240 − 360 cm are omitted as no retrieval was able to be made due to the highly saturated nature of the sample. The reported values are averaged over the depth they represent.

	Unit	Ditch Base	Ditch Bank			Site H		Site P		
Depth	cm	0 − 20	0 − 120	120 − 240	240 − 360	0 − 120	120 − 240	0 − 120	120 − 240	240 − 360
pH	—	5.9	8.0	7.7	7.2	9.5	9.9	8.6	7.6	7.5
N	%	0.55	0.07	0.12	0.04	0.04	0.07	0.05	0.08	0.09
C		7.1	2.8	7.1	4.5	2.8	2.9	3.0	5.2	6.0
OM		8.8	2.0	0.9	1.9	2.7	1.8	1.8	4.3	1.0
Free Fe Oxides		16.5	–	–	–	0.3	0.5	0.4	1.4	3.2
As	(mg kg^{-1})	13,300	89	2570	1260	440	900	17	410	185
Cr		60	30	30	20	120	50	35	160	13
Pb		360	525	11,250	13,210	1210	380	130	4310	1770
Fe		97,060	19,300	53,070	49,040	35,050	23,700	18,415	1,59,800	1,05,600
Mn		558	217	197	67	580	310	425	550	143
S		4157	649	3050	4120	2980	11,300	1600	7775	8150
Al		13,300	10,600	3660	2400	13,015	12,680	13,770	4620	2700

Table 2
Elemental composition of collected soil samples from the ditch (D1–D10) and riverbank (R1–R6). Di (i = 1−10) samples represent ditch soils, and Ry (y = 1−6) is riverbank soils. Sampling locations D1−D6 and D7−D10 are referred to as "ditch downstream" and "ditch upstream" locations, respectively, in the text. Concentrations are all reported in mg kg^{-1} except for Fe* concentrations that are reported in g kg^{-1}.

Soil	pH	N	C	OM	As	Cr	Pb	Fe*	Mn	S	Al
D1	6.2	0.29	4.38	8.5	59,700	30	1300	195	428	2400	10,200
D2	6.1	0.32	4.81	8.2	51,000	40	1900	179	498	2600	12,400
D3	6.3	0.36	5.39	8.3	36,200	50	1100	136	555	3200	18,400
D4	6.2	0.31	4.35	7.5	42,600	40	2000	161	395	2700	15,200
D5	6.1	0.35	5.26	8.5	59,000	40	1600	185	525	2800	14,600
D6	6.1	0.32	4.81	8.4	67,300	40	2300	216	465	2400	12,500
D7	6.3	0.45	7.29	9.2	5400	70	100	100	468	3300	22,000
D8	6.4	0.49	7.79	9.3	5000	70	100	101	656	3500	24,500
D9	6.3	0.54	8.68	10.0	3900	70	100	106	636	3700	22,800
D10	6.6	0.46	7.00	9.3	1900	130	200	59	1335	2,500	27,500
R1	6.8	0.12	4.38	2.1	800	50	8600	78	287	4700	13,200
R2	7.0	0.09	3.12	1.9	500	50	4800	64	360	2300	11,100
R3	6.9	0.10	4.27	2.0	800	50	14,000	101	321	6300	9400
R4	6.7	0.09	3.75	2.3	600	50	10,700	96	557	3900	9200
R5	6.6	0.12	3.90	2.6	500	50	7200	76	281	7800	13,000
R6	6.9	0.09	3.67	2.1	400	50	7000	73	372	3300	11,900

prepared as resin−embedded thin sections using the tailored "x26a" method by Spectrum Petrographics, Inc (Vancouver, WA, USA). Specifically, samples were prepared in low oxygen and low−temperature conditions, were 30 μm thick, double−polished on Suprasil 2a fused silica, and mounted with cyanoacrylate adhesive.

For XRF map generation, the XFM beamline uses Kirkpatrick–Baez (KB) mirrors to deliver focused X–rays (2–10 μm spot) with tunable energy using a Si(111) double crystal monochromator. Samples were oriented 45° to the incident beam, and the XRF detector (Canberra SXD 7–element SDD) was positioned 90° to the incident beam. For each sample, a large μ−XRF map (3 ×4 mm^2 or 4 ×4 mm^2) was obtained by raster scanning the sample in front of the microbeam using a Newport stage with a 10 μm step size and 50 ms dwell time per pixel for the course navigation maps, but a 2 μm step size and 200 ms dwell time per pixel were used for fine–resolution maps. The X−ray energy was set at 12,800 eV. After map collection, specific areas of interest or hotspots were selected for μ−XRD and μ−XANES acquisition. μ−XRF maps were processed using the GSECAR Mapviewer software from Larch [48]. Athena was used to process μ−XANES spectra [55]. Powder X−ray microdiffraction measurements were then carried out using a wavelength λ = 0.6888 Å (E = 18 keV). The beamline is equipped with a Perkin Elmer 1621 XRD flat panel detector. The XRD patterns were collected in the 2−36° 2θ range. The exposure time for each point was 30 s. The spot size for the μ−XRD was 10 × 10 × 30 μm. The 2D images were calibrated in Dioptis [53] using LaB_6 standard reference, and the 1D patterns were analyzed using the computer program Match! [46] in conjunction with the ICDD minerals database.

2.4. Desorption experiments

A stirred−flow technique was used to assess the potential release of As from ditch soils during SLR, using river water, seawater, and electrolytes under oxic conditions. The soil used in the desorption experiments, i.e., ditch base soil, Table 1, underwent a drying process in an anaerobic atmosphere. Three different types of water were used for the influent: natural river water (pH 7.2) sourced from the Christina River, natural seawater (pH 7.8) collected from the surface coastal waters of the Atlantic Ocean at Cape Henlopen State Park, DE, USA, and a 10 mM NaCl electrolyte solution buffered to a pH of 7 with a 5 mM MOPS pH buffer solution. More information on the water characteristics can be found in Table S.2. The natural waters were collected from the top 5 cm of the source using a peristaltic pump, stored at 4 °C in HDPE bottles, and used in the experiments within 2 weeks of collection. The rate of As desorption was measured over 36 h using a methodology adapted from [34,37,70]. The experimental setup comprised a 16 mL flow−through continuously stirred reaction chamber. Each experiment was conducted in duplicate, maintaining a 1:8 soil(dry):solution ratio, a mixing rate of 100 rpm, and a flow rate of 1 mL min^{-1}. Samples were collected in 5 minute (5 mL) increments under ambient atmospheric conditions. The concentrations of metals of interest (i.e., As, Fe, and Mn) in the effluent was subsequently analyzed via Inductively Coupled Plasma Optical Emission Spectrometry (ICP−OES, Agilent 7100, Agilent Technologies, Santa Clara, USA). This approach allows for exploring the potential release of As and its commonly binding metals (Fe and Mn) under different salinity conditions, providing insights into the dynamic interactions between soil and solution during simulated SLR scenarios.

2.5. Site hydrology and sea−level rise projections

Dominant hydrologic flow was determined with groundwater depth obtained by several previously installed monitoring wells (e.g., Fig. S.2) on and surrounding sites H and P (Fig. 6, panel a). As the site is tidally influenced, groundwater depth determination used data collected during similar tidal cycles [84]. The groundwater levels and tides were recorded from Oct 2014 to Jan 2016 at 15−min intervals. Our mean observed tidal levels were well correlated to groundwater levels for each tidal cycle (Fig. 6). We then added 0.1 and 0.5 m to the observed tidal levels to predict the groundwater level responses to future "low" SLR scenarios (SLR=0.1 m and SLR=0.5 m) in the state of Delaware [15]. Coastal inundation scenarios were mapped using the state of Delaware's digital elevation model-based bathtub-model coastal inundation maps [7]. This methodology provides a basis for anticipating hydrological changes, aligning observed tidal data with groundwater levels, and projecting responses to potential SLR scenarios at the site.

3. Results and discussion

3.1. Contaminated sites and ditch soil profiles

3.1.1. Bulk soil characteristics

Fig. 1 illustrates the variations in pH and the concentrations of As, Fe, and S with depth in soils collected from Site H and Site P. Site H soils consistently exhibited higher As concentrations compared to Site P across all depths. At the surface, for instance, As was an order of magnitude more concentrated at Site H compared to Site P. Through the soil profiles, As concentration showed a generally positive correlation with depth (R^2 values for As−depth correlation in sites H and P are 0.74 and 0.45, respectively) (Fig. 1a). This increase in As concentration with depth is anticipated, given that the top meter of soil was replaced in a remediation effort. Whereas the remediation of the surface soil was

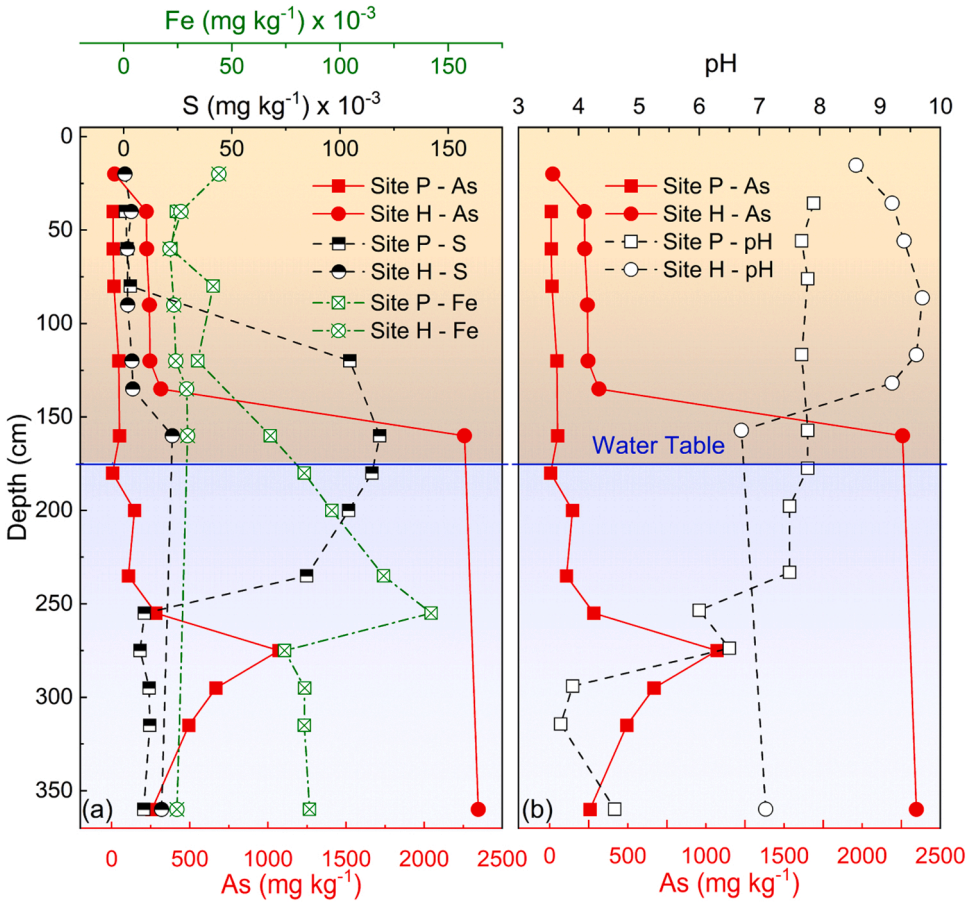

Fig. 1. Depth profiles of bulk soil As (lower x axis shown in red), Fe (top left x axis shown in green) and S (top left x axis shown in black) (Panel a) and pH (top right x axis Panel b) for sites H and P in 15−30 cm increments. Square and circle symbols represent Site P and Site H data, respectively. The horizontal blue lines show the average water table depth and the shaded blue area is where the soil is usually saturated. Data points are shown by symbols and lines show the moving average of the data points for discrete depths with a period of 2. Discrete depths were 50, 70, 100, 130, 150, 170, 190, 217, 245, 265, 285, 305, and 335 cm for Site P and 10, 30, 50, 75, 128, 147, 190, and 300 cm for Site H. The characteristics of Site H at 240−360 cm are not shown as no retrieval was possible for that depth due to the highly saturated nature of the sample.

completed by excavation and replacement with clean fill, elevated As levels persist at depth in both sites. The environmental hazards of these high levels of contamination are amplified because they are located within the saturated zone (i.e., below the average water table at 1.75 m), increasing the likelihood of contaminant plume migration from the original site of contamination. The concentrations of Fe and S remained relatively constant for Site H through the soil profile. At Site P, however, an elevated S and Fe zone existed from 1.3 to 2.2 m and below 1.5 m, respectively. Maximum S and Fe concentrations were measured at 1.5 and 2.5 m below the surface at Site P. Interestingly, the peak in As content occurred around the same depth as that of Fe at Site P (see Fig. 1a).

Sorption of As is highly affected by pH, and the pH of the soil profiles is considerably different at the sites (Fig. 1b). Site H had pH levels up to 9.9, which is rarely seen in soils and can be attributed to the legacy of contamination at this site. The pH did decrease through the soil profile, but only at 1.5 m below the surface, and the minimum value was a circumneutral 6.7 at 1.9 m below the surface. The zone in which the pH was at or above 9.0 is above the point of zero charge (PZC) for many soil minerals, and therefore, the soil has a net negative charge and thus contributes to low levels of sorption and subsequent high levels of anionic As release from Site H. In contrast, the pH at Site P followed a general decreasing trend as depth increased, with a maximum value of 7.9 at 0.5 m below the surface and a minimum of 3.7 at 3.1 m below the surface (Fig. 1b). These low pH values occur at the same depth as the increased soil As, which is due to the surge in As sorption on Mn and Fe oxides as the pH dips below the mineral's PZC (e.g., [56,25]).

The characteristics of the soil profiles collected from Site H and Site P were then compared to those of the ditch base and bank (Table 1). The ditch soil was acidic at the surface, while the bank and the Sites' soils were basic. Moreover, the OM, Fe oxide contents, and concentrations of As and S were considerably higher on the ditch base. Specifically, As concentration was an order of magnitude higher in the ditch base than in the bank and Sites. Higher OM content is expected when a soil system is more acidic because bacterial growth is restricted and OM decomposes more slowly under acidic conditions, leading to its accumulation in the soil [42,47]. Additionally, in the ditch, oxygen levels become depleted as waterlogged soil pores impede the diffusion of atmospheric oxygen into the soil. Wet, anaerobic conditions often lead to the accumulation of substantial amounts of OM, as decomposition occurs much slower in low-oxygen or anaerobic environments compared to oxygen-rich conditions. Furthermore, specific byproducts of anaerobic metabolism can be toxic to many microbial species, therefore acting as preservatives for OM [76]. This higher OM content can influence As cycling and mobilize or immobilize As when soils experience flooding and submerging [23]. Particularly, competition for sorption sites at Fe and Al oxide surfaces between humic substances and As [22,57,73,8] may render As more available in soils for redox transformations.

Ditch bank soils were about four times more contaminated with As compared to the Sites' surface soils (Table 1). Arsenic concentration in all soils consistently increased with depth, reaching its maximum at increments of 1.2−2.4 m below the surface. Even at deeper depths, the

soil along the ditch banks retained the highest As contamination levels among all the examined soils. This trend mirrored the pattern observed for Fe concentrations in the ditch bank and Site P soils, whereas Fe concentrations slightly decreased with depth at Site H. In contrast, S concentrations continuously increased with depth in all the samples. Site H soils exhibited the highest pH among the examined soils, while the ditch surface soils were characterized as acidic with a pH of 5.9.

3.1.2. *Depth profiles of solid−phase As K−edge XANES*

Fig. 2 shows As XANES spectra for the ditch surface soils and the soil profiles of the ditch bank, Site H, and Site P. The spectrum of the saturated ditch soils perfectly aligns with our As(III) standard (sodium arsenite). In contrast, the ditch bank, Site H, and Site P white line positions primarily correspond to that of the more stable As(V) species. However, a shoulder feature is present on the spectra of lower−depth samples, indicating a mixed oxidation state for these samples. The LCF results (Fig. 2, Panel c) confirm that the saturated ditch soil is predominantly (90%) composed of As(III), with the remaining portion being As(V). Above 1.2 m depths, the ditch bank, Site H, and Site P soils were approximately 90% As(V), exhibiting a similarity explained by the remediation efforts conducted above this depth. Moving down the soil profile, differences between the Sites become apparent. At intervals of 1.2−2.4 m, Site P and ditch bank were still mainly comprised of As(V) with no As−S contribution, while Site H was composed of over 50% As

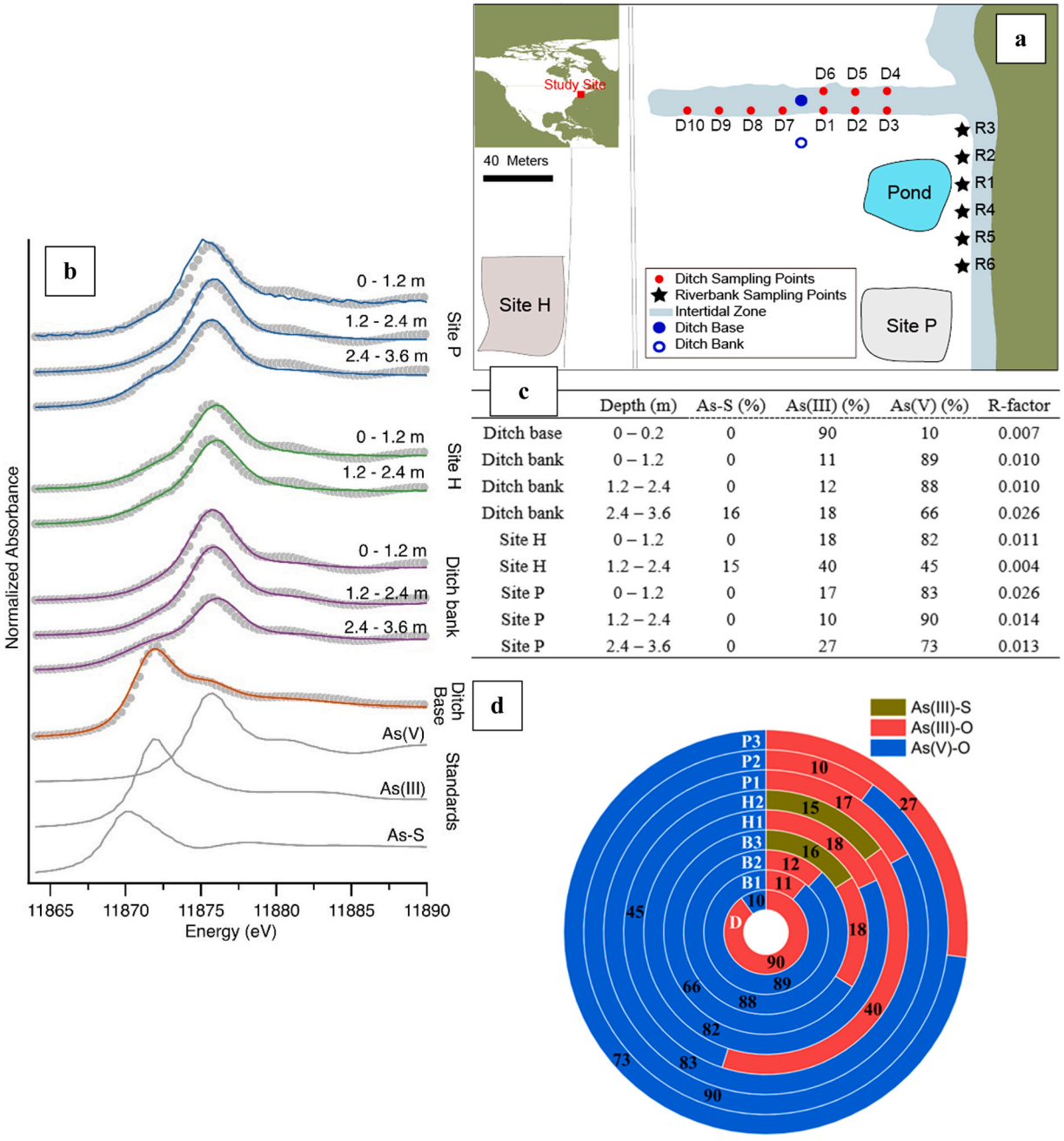

	Depth (m)	As-S (%)	As(III) (%)	As(V) (%)	R-factor
Ditch base	0 – 0.2	0	90	10	0.007
Ditch bank	0 – 1.2	0	11	89	0.010
Ditch bank	1.2 – 2.4	0	12	88	0.010
Ditch bank	2.4 – 3.6	16	18	66	0.026
Site H	0 – 1.2	0	18	82	0.011
Site H	1.2 – 2.4	15	40	45	0.004
Site P	0 – 1.2	0	17	83	0.026
Site P	1.2 – 2.4	0	10	90	0.014
Site P	2.4 – 3.6	0	27	73	0.013

Fig. 2. Arsenic XANES spectra of Site P, Site H, and the ditch base/bank soils at different depths (Panel b). The standards are shown in black, and the ditch base, ditch bank, Site H, and Site P spectra are shown in orange, purple, green, and blue, respectively. As(III), As(V), and As–S are the standard spectra for sodium arsenite, sodium arsenate, and realgar. Solid lines represent data and standards, and the grey dotted lines represent the fits obtained by LCF results (represented in Panel c). Panel a show the location of all sampling points (represented in Panel c). Percentages of As(III)−S, As(V)−O, and As(III)−O species are represented in Panel d in olive, blue, and red, respectively. The values are calculated from the LCF results (Panel c).

(III) (including As−S) (Fig. 2). Below 2.4 m at Site H, sampling was impractical due to saturation. Nevertheless, given the water table's position (1.75 m), it is assumed that reducing conditions at this depth create an environment conducive to As−reducing processes at the Site. Below 2.4 m, a significant shift in the ditch bank As composition occurred, with As(III) increasing to 18%, and the appearance of As−S species comprising 16%. At this depth, the ratio of As(III) to As(V) was 30 to 70% at Site P.

The speciation of As in both the ditch bank and Site P remained consistent from the surface to a depth of 2.4 m, primarily comprising the less mobile As(V) species. Below 2.4 m, evidence of As reduction was observed at both locations. This suggests that As from Site P is not substantially migrating to the drainage ditch. Site H, however, showed a significant shift to more reduced As speciation below 1.2 m, and the reduction occurred to a greater extent at this location and depth than at either of the other sites. As(III) is more mobile and toxic than its pentavalent counterpart As(V) in the environment [45,56,63,64]. Therefore, its greater contribution to As composition at near−surface soils in Site H can correspond to increased release of As into solution, which in this case is the surrounding groundwater. This indicates that the reducing groundwater carries As and Fe ([84], Fig. 6 a), most probably from Site H where As is more mobile, and mixes with oxic water at the ditch bank/base where As oxidizes to As(V). Additionally, under prolonged reducing conditions with sufficient S concentrations, As can be removed from solution via precipitation into authigenic sulfide minerals, such as orpiment or realgar, and/or as a trace component in Fe sulfides, such as mackinawite ([13,35,49]). Arsenic−sulfide species formed at both the ditch bank (2.4–3.6 m depth) and Site H (1.2–2.4 m depth; Fig. 2). These As−S and As−Fe−S species are relatively more stable than other As(III) species, but a shift in redox conditions from reducing to oxidizing (as explained in Section 3.4 and Fig. 7) may lead to oxidative dissolution of the authigenic As sulfides and As associated with Fe sulfides.

3.2. Detailed soil properties at the ditch and riverbank

3.2.1. Ditch and riverbank soils characteristics

Table 2 outlines the comprehensive physicochemical properties of soils D1−D10 and R1−R6, revealing substantial variations in total metal composition between soils from the ditch and riverbank and the heterogeneity in the area. Soil samples taken from the ditch area exhibited elevated average concentrations of Cr (60 mg kg^{-1}), As (33,000 mg kg^{-1}), and Pb (1,500 mg kg^{-1}) (Table 2). In comparison, the mean concentrations of Cr and As were relatively lower at 50 and 600 mg kg^{-1}, respectively, while Pb concentrations (8,700 mg kg^{-1}) were considerably higher in the riverbank soils. Typical concentrations of Cr, As, and Pb are reported as 5–30 mg kg^{-1}, 1–10 mg kg^{-1}, and 30–100 mg kg^{-1} in Delaware soils, respectively [38]. It is evident that the soil samples from the study area surpass these regional averages by orders of magnitude, particularly for As and Pb. Furthermore, the average concentrations of Cr in the soils also exceedes the State's average, indicating an overall elevated contamination level in the investigated area.

The spatial distribution of As exhibited heterogeneity within the ditch soils, with noticeably elevated contamination downstream of the ditch, particularly in samples D1−D6 closer to the riverbank. Conversely, Cr and S concentrations were higher upstream of the ditch. Visual observation indicated groundwater flow, predominantly downstream in the ditch. As highlighted in earlier sections, the increased contamination downstream of the ditch is attributed to groundwater transporting As from Site H; the possible primary As source in specific sections of the ditch. Therefore, the heterogeneity in As distribution can be attributed to the groundwater acting as an As source in some parts of the ditch. Ditch soils were 55 times more enriched in As and 17%, 40%, 70%, and 60% more contaminated with Cr, Ni, P, and Zn, respectively, compared to the riverbank soils. Riverbank soils, on the other hand, were 10 and 40 times more contaminated with Pb and Cu, respectively, and 25%, 50%, and 62% more enriched in Cd, Co, and S than the ditch soils. Sorption of As is affected by pH and the pH of the ditch and riverbank soils does not vary greatly and is about neutral. Redox potential variations throughout the soil profiles of the ditch base and bank were measured and discussed in detail by [84]. Briefly, soil redox showed a bimodal depth profile. Closer to the surface, tides caused fluctuations between reducing/oxidizing conditions while the soil was always saturated below 2.0 m and in a reducing condition. Soil texture primarily consisted of loam, with some sandy loam zones observed in both ditch and riverbank soils. The inhomogeneity was observed again in the ditch soils characteristics with lower pH and higher OM and total nitrogen content noted upstream of the ditch (refer to Table S.1). These heterogeneities in the physicochemical characteristics contribute to the complex dynamics of contaminant behavior in the studied areas.

3.2.2. Bulk As−XANES analysis of the ditch and riverbank soils

As shown in Fig. 3, As speciation using XANES analysis displayed a mixture of As(III) and As(V) species along the ditch and riverbank. References used for the XANES LCF included laboratory–synthesized and natural minerals (Table S3). Detailed LCF results representing standards that best reconstruct the sample data are reported in Fig. 3, Panel c, and the percentages of major As species are shown in Fig. 3 Panel d. Analysis of soils from the ditch downstream (D3, D4, and D5) indicates an average composition of 63% As(III), with a portion appearing as As_2S_3. The presence of As−S species is further evidenced by the pre−edge feature around 11871 eV in the spectra of D3−D5 soils (Fig. 3). Oxidative dissolution of As sulfide species can, therefore, be a pathway for water pollution with As, when reduced soils be oxidized.

Arsenite species tend to be more weakly bound to soils and sediments and, therefore, would be more mobile than As(V). The groundwater flow at the area where As(III) species are detected in the ditch soils (Fig. 6 a) suggests that these species may originate from Site H and be carried by groundwater to the ditch. These mobile and toxic As species can either be stabilized by conversion to As−S or As(V) species or find their way into the Cristiana River during diurnal and seasonal hydrological fluctuations, as well as different SLR scenarios. The considerable contribution of As(III) and As−S species in the riverbank soils shows that the As (III) species are migrating even further seaward. Upstream ditch soils comprised 30% arsenite and 70% arsenate, while the ratio shifted to 40−60% in the riverbank soils. At the riverbank, R1 and R2 exhibited 14% and 2% As−S species, respectively. Arsenate species generally bind to Fe oxides through an inner sphere surface complex, while As(III) can be adsorbed through an inner and outer sphere surface complex [28,62]. Therefore, our results show that As oxidation state varies considerably in the ditch and riverbank soils, which implies differences in potential As mobilization pathways.

3.2.3. Elemental distribution, micro X − ray absorption spectroscopy, and XRD analysis of the ditch and riverbank soils

The μ–XRF maps in Fig. 4 illustrate the distribution of As, Fe, Mn, and Cr in soils D2, D7, R3, and R4. For a more comprehensive understanding of the speciation and mineral phases involved in the retention and release of different As species, specific hotspots were subjected to additional analysis using μ-XANES and μ-XRD (refer to Fig. 4, Fig. S7, Table S4). The μ–XRF maps of ditch soils reveal areas where As is associated either with Fe and/or Mn or exists as discrete, highly concentrated As hotspots. Color−coded maps and As Ka intensities per pixel over the Fe and Mn Ka intensities (see Figs. S.3, S.4, and Fig. 4) suggest a strong correlation between As–Fe and As–Mn in the ditch soils. The average R^2 values for As−Fe and As−Mn associations are 0.80 and 0.65, respectively. This correlation aligns with the existing literature [43,30,32,74,24]) and indicates strong As–Fe and As–Mn associations.

The μ–XANES spectra obtained from soil samples D2 and D7 indicate a mixture of As(III) and As(V) at the hotspots in these soils. In some spots (e.g., spot 10 in D2 and spots 5 and 9 in D7), a sharp white line at

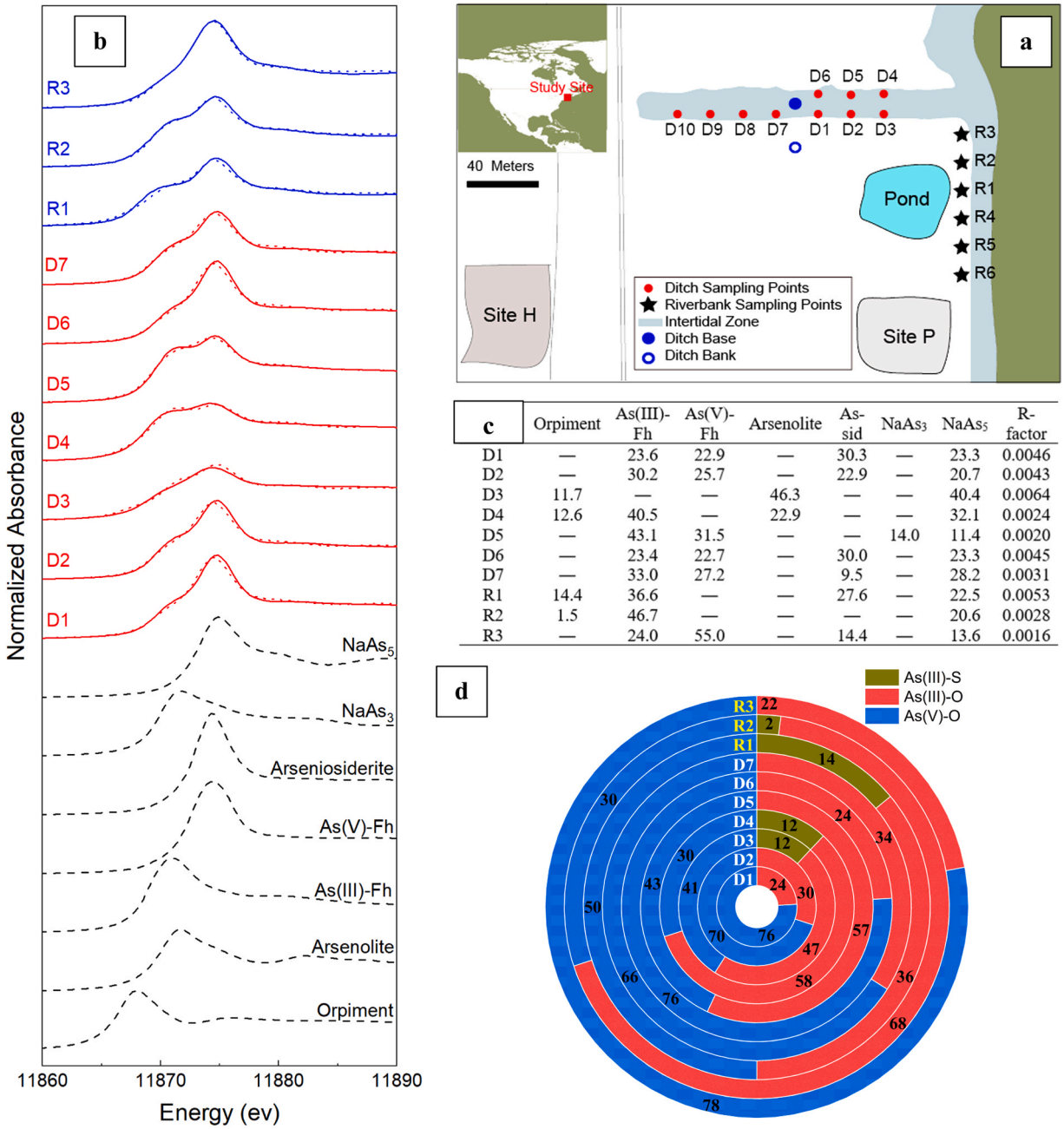

c	Orpiment	As(III)-Fh	As(V)-Fh	Arsenolite	As-sid	$NaAs_3$	$NaAs_5$	R-factor
D1	—	23.6	22.9	—	30.3	—	23.3	0.0046
D2	—	30.2	25.7	—	22.9	—	20.7	0.0043
D3	11.7	—	—	46.3	—	—	40.4	0.0064
D4	12.6	40.5	—	22.9	—	—	32.1	0.0024
D5	—	43.1	31.5	—	—	14.0	11.4	0.0020
D6	—	23.4	22.7	—	30.0	—	23.3	0.0045
D7	—	33.0	27.2	—	9.5	—	28.2	0.0031
R1	14.4	36.6	—	—	27.6	—	22.5	0.0053
R2	1.5	46.7	—	—	—	—	20.6	0.0028
R3	—	24.0	55.0	—	14.4	—	13.6	0.0016

Fig. 3. Arsenic XANES spectra of the ditch (D1–D7) and riverbank (R1–R3) soils (Panel b). The standards are shown in black and the spectra for the ditch and riverbank soils are shown in red and blue, respectively. As(III)–Fh, As(V)–Fh, and As(V)–Go are the standard spectra for the corresponding As species adsorbed on ferrihydrite (Fh) or goethite (Go). Data and standards are represented by the solid and dashed lines, respectively. The fits obtained by LCF results (represented in Panel c) are shown by dotted lines. Panel a show the location of all sampling points (represented in Panel c). Percentages of As(III)−S, As(V)−O, and As(III)−O species are represented in Panel d in olive, blue, and red, respectively. The values are calculated from the LCF results (Panel c) reported in the figure.

11875 eV, lacking humps before and after the white line (orange and gray stripe), is characteristic of As(V) adsorbed to Fe oxides XANES standard spectrum (e.g., [68]). However, in spots 1, 3, 4, and 9 in D2 and spots 3, 10, and 12 in D7, a hump is observed at about a fifth of the height of the white line. Additionally, spots 5, 6, 7, 8 in D2 and 1, 2, 6, 7, 8, and 10 in D7 display humps at approximately half the height of the white line, around 11871 eV (orange stripe in Fig. 4). These features resemble the XANES spectrum of As(III)–bearing goethite and ferrihydrite [68].

It is important to note that D2 and D7 are situated near groundwater discharge areas in the ditch, where groundwater may serve as the source of As(III) in these soils. μ-XRD patterns confirmed the presence and dominance of Fe−oxides in ditch soils, consistent with the μ–XANES data. Besides Fe−oxides, As oxides such as arsenolite and claudetite contributed to most spots scanned in the ditch sediments (see Table S4). The main mineral phases in sediment D2 were arsenolite (As_4O_6), goethite ($\alpha - Fe^{3+}O(OH)$), manganese oxide (Mn_2O_3), and periclase (MgO). Sediment D7 was composed mainly of arsenolite (As_4O_6), claudetite (As_2O_3), and iron oxides such as maghemite ($\gamma - Fe_2O_3$) and magnetite ($Fe^{2+}Fe_2^{3+}O_4$). Some spots in D7 were comprised of minerals containing Fe−S, Zn−S, and Mg−O. Arsenolite and claudetite, mainly found in these soils, are products of As−S oxidation [51].

In riverbank soils, micro XRF maps did not demonstrate a strong correlation between As–Fe and As–Mn (see Figs. S.5 and S.6). However,

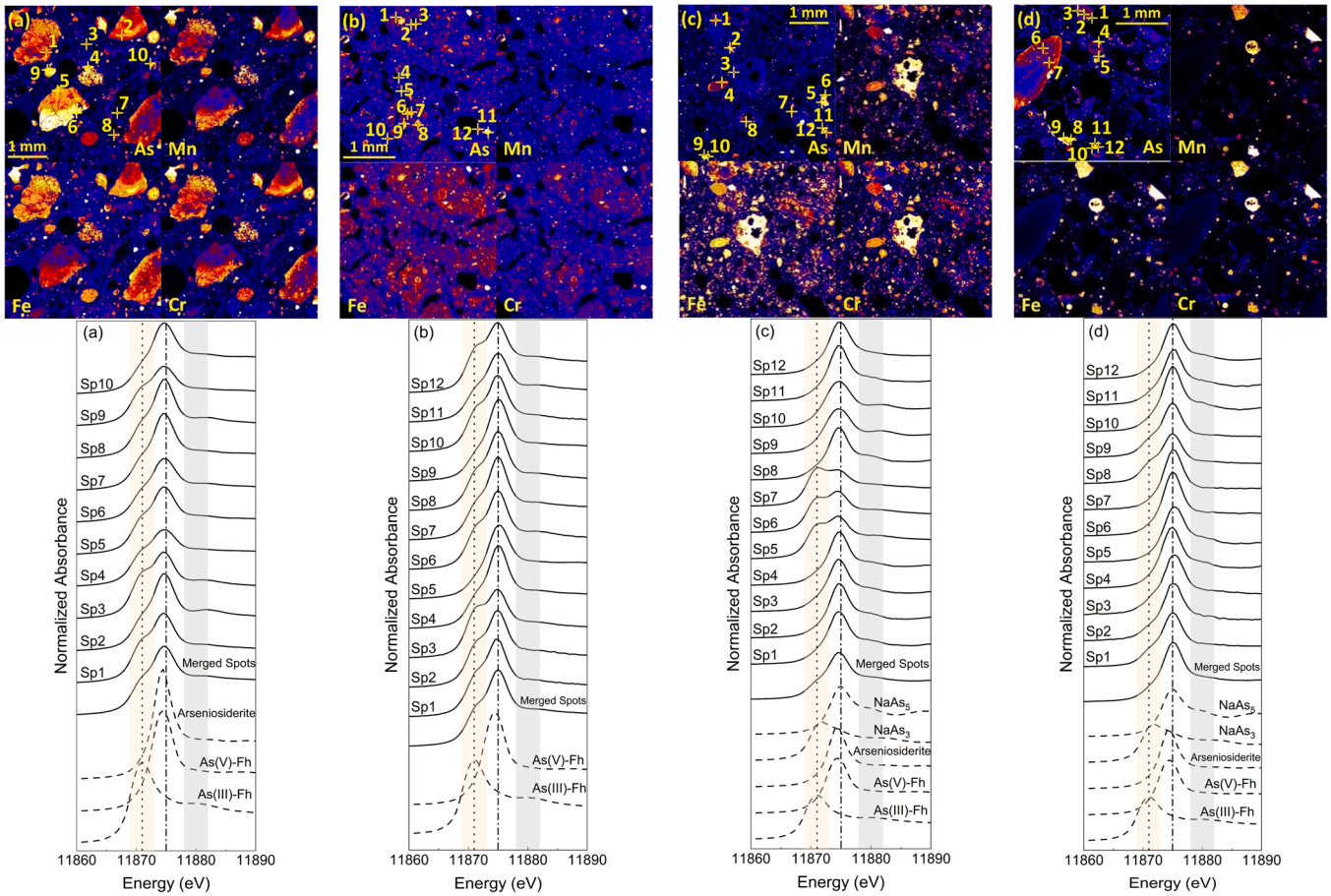

Fig. 4. The micro−scale spatial distribution of As, Mn, Fe, and Cr in soils (a) D2, (b) D7, (c) R3, and (d) R4. Different hotspots were selected and analyzed using μ−XANES (Fig. 4) and μ−XRD (Figure S.7). In each top big square at panels a-d, starting from the 12 o'clock position and moving clockwise, the distribution of Mn, Cr, Fe, and As are shown in four smaller squares.

Cr displayed a strong association with Mn and Fe in these soils. The inflection points of the first derivative of As μ–XANES spectra in the riverbank sediments, positioned at about 11875 eV (Fig. 4(c, d)), indicate the presence of As(V) in all hotspots analyzed. Overall, riverbank soils' hotspots had less As(III) than the ditch. Some exceptions, like spots 6, 7, and 15 in R1, spots 5, 6, and 7 in R3, and spot 8 in R4, exhibited humps characteristic of As(III) species. XRD data revealed that riverbank soils (R3 and R4) primarily consist of Fe−oxides such as hematite (Fe_2O_3), maghemite ($\gamma - Fe_2O_3$), (para)scorodite ($FeAsO_4{\cdot}2\,H_2O$), and goethite ($\alpha - Fe^{3+}O(OH)$), and S−containing minerals such as jarosite ($KFe_3(SO_4)_2(OH)_6$), realgar (As_4S_4), and orpiment (As_2S_3).

The absence of features at the high−energy side of the white line (gray stripe) in most μ–XANES spectra presented in Fig. 4 indicates that the majority of As in these hotspots is not structurally bound within crystalline phases [38]. This implies that a significant portion of As in these soils may be more susceptible to release into the solution during exposure to anoxic conditions, as compared to situations where As is sequestered within more ordered phases. However, this finding is incompatible with our sequential extraction results, which indicated that the majority of As is in the occluded phase [39]. Despite the micro−scale heterogeneity depicted by the data, there is overall agreement between the micro and the bulk data suggesting the presence of different mineral phases containing both As(III) and As(V) in the soils, with some of these phases containing Fe and Mn. However, it is noteworthy that the μ−XANES data of the riverbank soils did not reveal As−Fe and As−Mn associations observed in the bulk analysis. Our μ−data also did not confirm our bulk sequential extraction results. This discrepancy suggests potential micro−scale variations that are not fully captured by the bulk analysis, emphasizing the importance of micro−scale investigations to understand localized variations in As speciation within the broader soil context.

3.3. *Effects of salinity on As release*

Fig. 5 shows the percent As release (panel a) and the concentrations of released As, Fe, and Mn (panel b) during the desorption experiments. About 86% of the total As in the ditch base soils was sequestered within hydrous oxides, while the remaining 13% was attributed to inner−sphere and 1% to outer−sphere As sorption [39]. Upon subjecting the soil to a 36−hour reaction with natural river water and seawater, the results, illustrated in Fig. 5, revealed the release of all exchangeable (outer−sphere complex) and a fraction of the oxide−sorbed (inner−sphere complex) As. The As release was the highest using NaCl, followed by river water and seawater inundations (Fig. 5, panel a). Desorption with river water resulted in the release of 4.74% of the total soil As, while desorption with seawater released 3.85%, indicating that river water led to a 22% higher As release compared to seawater (70.7 μg and 57.3 μg, respectively). The most substantial As release, approximately 6% of the total As after 36 h of reaction, occurred during desorption with NaCl solution. As seen in Fig. 5, panel b, As release was sharp and abrupt soon after the introduction of the saline solutions. About an hour after the salinity was introduced, a decline in aqueous As concentration was, however, observed before it reached a plateau almost 12 h later. Importantly, all As concentrations were orders of magnitude higher than the EPA and WHO thresholds for As in drinking water (Fig. 5, panel b). Higher As release was always accompanied by higher Mn and Fe

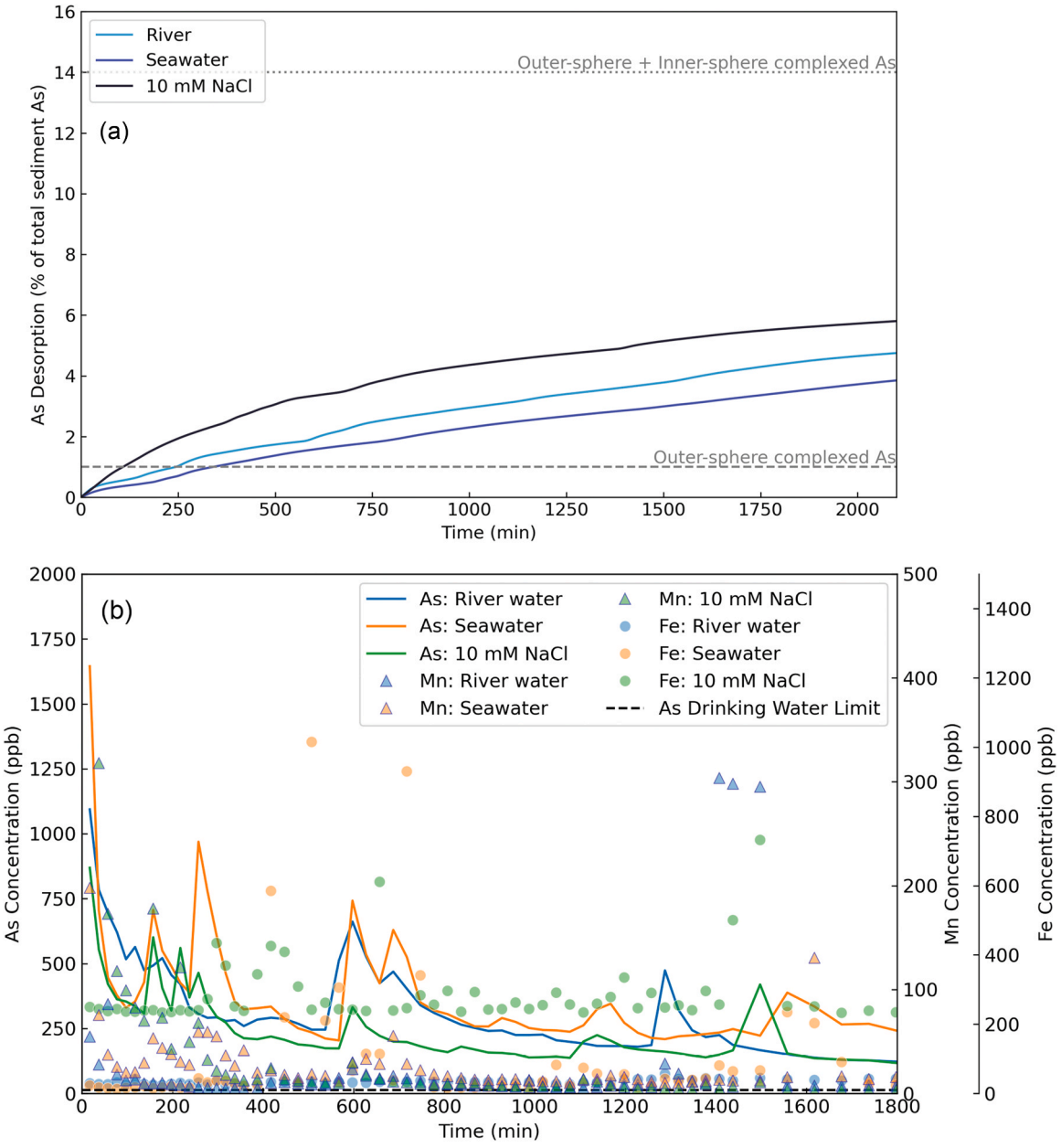

Fig. 5. Arsenic release over 36 h reaction time is shown as a present of total As in the ditch soil in panel a. Percent As release is under oxidizing conditions in natural river water and seawater and its desorption in 10 mM NaCl. Black, blue, and purple in panel a indicate the release of As in 10 mM NaCl, river water, and seawater. Panel b shows the concentrations of As, Mn, and Fe in the solution at different inundation scenarios during the first 30 hours of the desorption experiments. The black dotted horizontal line shows the EPA acceptable concentration for As in drinking water (10 μg L^{-1}).

concentrations in the solution indicating that Fe/Mn dissolution contributed to As release. However, low Fe and Mn release indicates that other parallel mechanisms acted in concert with the dissolution to release As (Fig. 5, panel b).

Interestingly, despite the significant As content found in the ditch soil (specifically, 13,300 mg kg^{-1}, as shown in Table 1) and the prevalence of As(III) comprising 90% of the soil As (as depicted in Fig. 2c), our experiments revealed that less than 10% of the As was desorbed from the ditch. It is worth noting that the desorption data align well with the sequential extraction data indicating that only a small fraction of As is in the readily released forms. This highlights that the partitioning of different As species in soil phases acts in concert with As speciation to define the behavior of this redox-sensitive element in dynamic environmental scenarios. The desorbing solutions used in this study mainly release As from the exchangeable and quickly mobilized fractions. A significant portion of As in this soil is, however, in the residual phase or is associated with highly crystallized Fe and Mn oxides. As a result, the release of a considerable amount of As from the ditch is hampered due to occlusion within these phases which are stable under the oxidizing conditions of this desorption experiment (Fig. 5, Panel b). Despite the relatively small release of As from the ditch soil (compared to the original As content of the soil), the final concentrations of released As using different desorbing agents significantly exceeded the US EPA standard for As in drinking water (10 μg L^{-1} Fig. 5, panel b). Furthermore, our experiments were conducted under oxidizing, circumneutral conditions over a relatively short period (36 h) to match the environmental conditions of the ditch soil and its tidally–influence environment [84]. However, it is likely that more extensive As release could occur in different environments, such as reducing or acidic conditions, or with extended reaction times (e.g., [39]).

The increase in salinity is expected to increase the mobility of metal (oid)s and trace metals due to dispersion and increased competition for sorption sites from increased cations and anions [23,85]. Competition of seawater cations with H^+ and Al^{3+} in soil surface can also lower the pH, influencing surface charge and, consequently, sorption reactions [79,80,81]. Additionally, the rise in salinity is anticipated to decrease the binding of metals to humic acids, as noted by Du Laing et al. [23]. This, coupled with the formation of soluble chloride complexes, contributes to an increased release of As. More As release in river water inundation scenario in this study, however, suggests that complexation and ionic exchange reactions may not be the primary factors influencing the release of As from the studied soil. The fact that only 1% of the total As in the soil samples is distributed in the exchangeable fraction, makes As less susceptible to release through processes like ion−exchange or pH changes. Furthermore, in reducing environments, the presence of a high sulfate content in seawater followed by the precipitation of sulfide minerals can reduce the availability of metals, including As, through reduction of As(V) and precipitation of As(III) in sulfide phases [10,23,49,54,58,59] . However, sulfide can also react with As−bearing Fe oxides, resulting in oxidized S and dissolved ferrous Fe (e.g., [16,59,52]). Moreover, reductive dissolution of Fe oxides can increase when sulfate reduction occurs at basic pH, where Fe reduction rates can be limited by thermodynamic controls (e.g., [9,50]). In cases where S is abundant, on the other hand, SO_4^{2-} can potentially stabilize As−bearing hydrous oxides by forming bidentate binuclear ligand complexes [66]. When pH is above 5, elevated SO_4^{2-} is found to inhibit dissimilatory As(V) and Fe(III) reduction [11,14,36,78]. The use of oxic condition in conducting desorption experiments potentially eliminates the mechanisms described for As–S interactions in anoxic conditions. However, the concurrent As, Fe and Mn release to the solution, as observed in Fig. 5b, indicate that Fe/Mn oxide dissolution is likely to be contributing to As release in these experiments. Therefore, it appears that competition for surface sites (for exchangeable As fraction) and Fe/Mn dissolution (for non–exchangeable As fraction) are the main factors governing As behavior in this study. Further research into the role of SO_4^{2-} on As and Fe cycling throughout a shifting redox potential can help with narrowing the window of possible mechanisms at each specific environmental condition.

It is worth noting that previous literature has reported lower metal release in saline environments with high salt concentration (e.g. [67,39]). However, there are contrasting findings by e.g., [5,6,60] , which suggest higher release of metals in seawater inundation scenarios. Sricharoenvech et al. [67] investigated Cr release from contaminated urban coastal soils under aerobic and anaerobic inundation scenarios using artificial seawater (ASW) and artificial river water (ARW). They found lower Cr release in seawater inundation, attributed to the minimal contribution of exchangeable Cr in the soil sample. Conversely, the highest Cr release occurred in freshwater inundation under oxic conditions, leading to the conclusion that soil redox conditions primarily govern Cr release rather than ion exchange or pH changes. Sanchez [60] examined As(V) desorption from goethite and ferrihydrite using ASW and ARW. They consistently observed slightly higher As(V) desorption in ASW due to adsorption competition between SO_4^{2-} and As(V) for available sorption sites. LeMonte et al. [39] studied the effects of natural seawater and river water inundation on As mobilization and speciation across predefined Eh zones using historically As−contaminated soils. They found that river water resulted in approximately twice as much As release compared to seawater, primarily attributed to the impacts of the seawater sulfur on As cycling in reduced soils and sediments. In batch studies on As(V) desorption from ferrihydrite using ASW solutions with different salinity levels, Barreto et al. [5] found that $<$ 1% As(V) desorbed by 1% ASW, with about 8% desorbed at 100% ASW. Although the release was less than 10% even at the most saline inundation scenario, the amount of released As(V) gradually increased with increasing salinity due to increased pH, changes in surface charge, and increased competition of anions for available surface sites. In their 2024 study on the impacts of salinity on chromate desorption from hematite [6], Barreto et al. found that ASW desorbed 20% more Cr(VI) even at just 1% concentration due to increased pH and the introduction of competing anions.

Comparing these findings with the current study sheds light on critical insights into the impacts of salinity on metals dynamics in the environment. Studies conducted on natural soils where microbiological processes act alongsidephysicochemical reactions, such as this study and those by LeMonte et al. [39] and Sricharoenvech et al. [67], show higher metal release in less saline inundation scenarios. This suggests that higher osmotic stress from increased salinity on the microbial community may hinder metals release in seawater inundation scenarios. Conversely, abiotic studies on synthesized minerals and artificial water systems, as demonstrated by Barreto et al. [5] and [6] and Sanchez [60], show that competition for sorption sites and electrostatic forces govern As release in the absence of microbes, resulting in higher release with increased salinity. Further investigation into the interplay between microbiological and geochemical cycling of As under different salinity and redox scenarios is needed to better understand the mechanisms involved in As behavior during SLR events.

3.4. Site hydrology

Panel a in Fig. 6 illustrates a range of SLR inundation scenarios at the study site. The results show that the ditch and riverbank area are prone to flooding even at SLR= 0.3 m. Conversely, Site P will remain above water, even at SLR= 1 m, while certain sections of Site H experience inundation at this level. These sites exhibit elevated As concentrations at the surface, which further increase with depth. Particularly in the ditch and Site H, As speciation analysis reveals a significant contribution of the mobile As(III) in these soils that are prone to release even at the current hydrological patterns without river water and seawater exposure. It is essential to recognize that changes in sea levels will not only impact the surface characteristics of these soils but will also alter the elevation of the water table, consequently influencing the geochemical conditions within the soil profiles. As highlighted in Section 3.3, reaction with river water is anticipated to enhance As release from the surface and depth of the soils at these sites. Additionally, the alkaline conditions prevailing in Site H are expected to contribute to even more As release when submerged.

The rising sea levels not only cause the As plume center to migrate inland but also increase the overall range of the plume migration, as shown in Fig. 6, panels b and c. Under stable sea level conditions, the plume moved only 5.0 m in 15 months [84]. However, with a 0.1−meter SLR, the landward movement of the plume can double, expanding to 10.0 m (see Fig. 6, panel b). The average movement distance of the plume also significantly increases, reaching 17.6 m in the scenario of a 0.5−meter SLR. Past records suggest that the extent of the migration range of the As plume typically falls within 3.5−6.3 m [84]. Nevertheless, with a mere 0.05 m SLR, the migration range widens to 5.4−9.5 m. Elevating the SLR to 0.1 ms further extends the migration range to 7.8−13.7 m, and under the more extreme condition of a 0.5−meter SLR, it significantly broadens to 14.1−23.2 m. This dynamic shift in hydrologic patterns compounded by altered geochemical condition can lead to severe As release. Moreover, there is a higher risk of upward migration of subsurface As compounds through advection, as capillary forces in the vadose zone move groundwater toward the surface.

The SLR−induced inland forcing of the contaminated As plume can also increase the saturation of currently unsaturated contaminated soils in the vadose zone of Sites H and P. Such a change in redox conditions can cause the mobilization of Fe (hydro)oxide−bound As through the reductive dissolution of the Fe (hydro)oxide phases. Sea−level rise can lead to anoxic conditions where oxidized As on metal oxides can be mobilized as the oxides reductively dissolve (Fig. 7, Panel a). On the other hand, in the oxidation of anoxic soils resulting from water

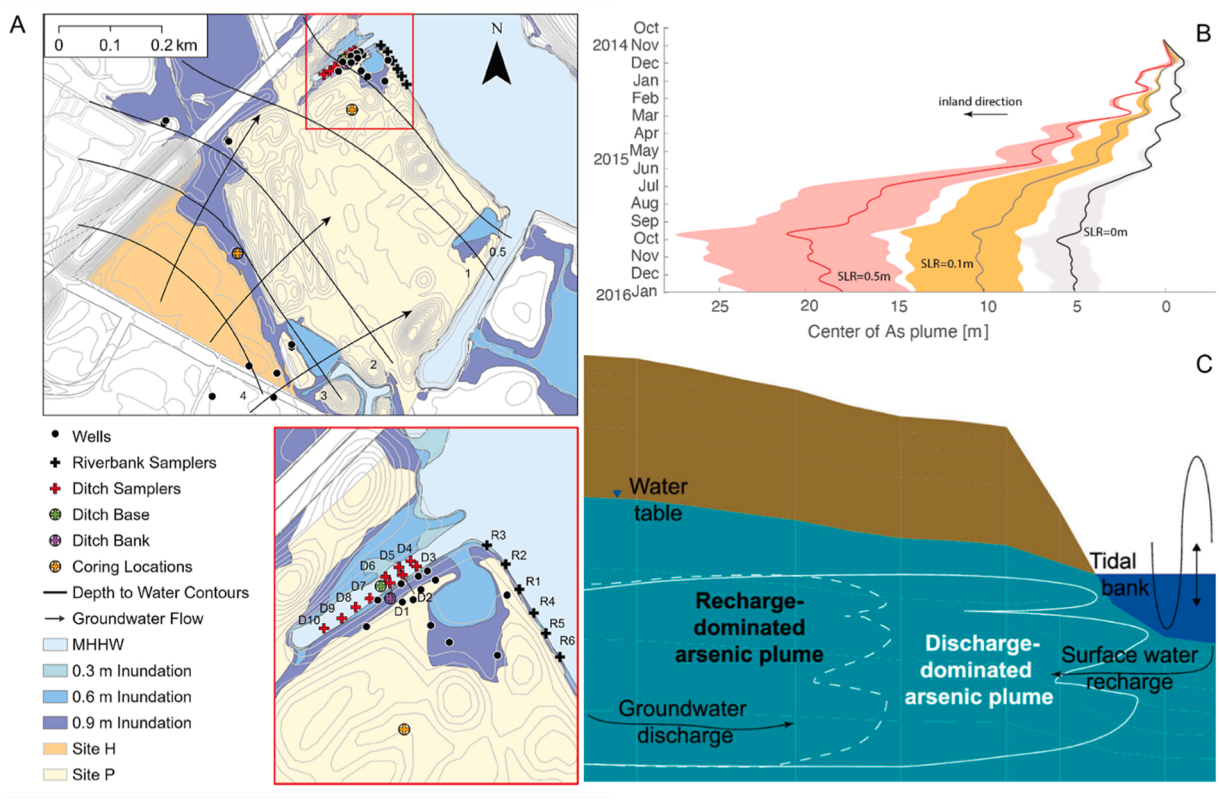

Fig. 6. Location of the sampling sites, groundwater flow direction, and the projection of 0.3 m, 0.6 m, and 0.9 m SLR scenarios (Panel a). MHHW stands for the mean higher high water. Panel b shows the hydrologic control on the movement of the As plume under different SLR scenarios (SLR=0 m: history, SLR=0.1 m, and SLR=0.5 m). Solid lines indicate mean, and the shades are 25 – 75% movement. Panel c shows the impacts of hydrological patterns on As plume near the ditch (from [84] with permission).

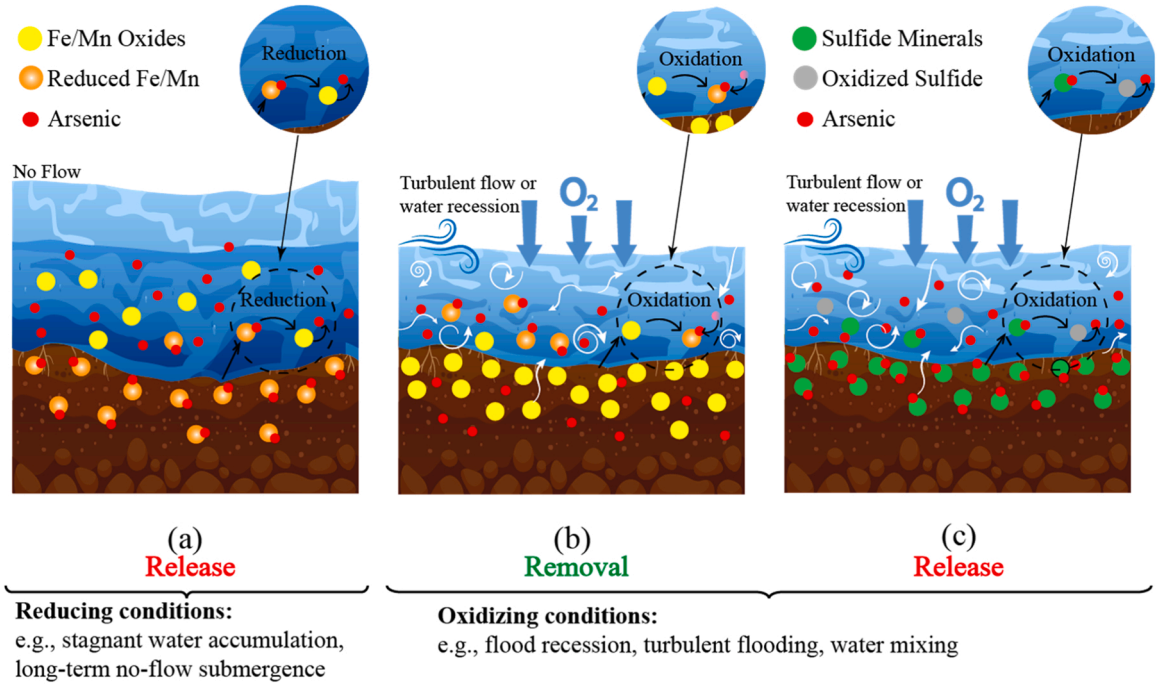

Fig. 7. The oxidation/reduction processes acting on As associated with the iron oxides, manganese oxides, and sulfide minerals in the soils during hydrological shifts associated with flooding and SLR.

recession or turbulent flooding, high-surface-area solid-phase Fe and Mn oxides can form by reacting reduced metals with dissolved oxygen to scavenge As from the dissolved phase, hence reducing As availability (Fig. 7, Panel b). Alternatively, such oxic conditions may also mobilize the As stored in sulfides via oxidative release as shown in Fig. 7, Panel c. The adverse effect of salinity on As sorption, as observed in the desorption experiments (Section 3.3), is relevant to and will combine with the mechanisms mentioned here.

4. Conclusion

In this study, the soil samples collected from an urban coastal area in Wilmington, DE, had extremely high concentrations of As (1 −6%). Despite the high As concentrations in the soils, only a small percentage (1%) was present in the exchangeable fraction. However, desorption experiments conducted using natural river water, seawater, and electrolyte solutions resulted in a release of As in quantities considerably higher than the US EPA and WHO standards for As in drinking water. Even though the level of As contamination in these soils was very high, they represent the amount of As content found in industrially-impacted environments. Moreover, most of the As in these soils were not exchangeable. Therefore, the findings of this study are relevant to other locations with similar biogeochemical characteristics and climate−related stressors, where the levels of As in shallow soils and sediment may not be as extreme, but As is more present in exchangeable forms.

The strong correlation observed among As, Fe, and Mn in the studied soils strongly suggests the sorption of As to Fe and Mn oxides. The predominant sorption to Fe and Mn oxides indicates that As in these soils could potentially desorb from Fe(III) oxides should these phases undergo reduction under anoxic conditions. This scenario could become plausible if the nearby Christina River floods the area, leading to changes in environmental conditions. Therefore, despite the remedial actions taken in 2005, which involved excavating the ditch, capping the soils, and constructing a berm between an adjacent stormwater pond and the ditch to prevent potential soil transfer, the area continues to pose an environmental threat, especially when SLR occurs. Our hydrological data further suggest that the expected rising sea levels not only cause the present As plume center to migrate inland but also increase the overall range of the plume migration.

Results obtained from our synchrotron–based spectroscopy suggest a mixture of As(III) and As(V) are present in the studied site. In current hydrological patterns, the ditch soils are in oxidizing condition at the surface (0−0.5 m) and always saturated below 2 m (Eh ~ −200 mv). The oxidizing environment promotes the prevalence of less mobile As(V) species in the surface soils of the ditch and riverbank. Consequently, the likelihood of reductive dissolution of Fe/Mn oxides and subsequent As release from surface soils is low under the present hydrological patterns. At different SLR scenarios, however, surface soils are expected to become reduced, leading to the reductive dissolution of Fe/Mn oxides and the release of As. Sulfate reduction is also not expected to considerably alleviate As release in this freshwater system. At deeper profiles, where reducing conditions is experienced and As(III) is more dominant, As release from the soils to groundwater is expected even during the current hydrological patterns. In some parts of the ditch where groundwater flow was reported, As−sulfide species that are more stable than As(III) were present. However, changes in oxidation levels due to SLR from reducing to oxidizing during turbulent flooding events or flood recession periods when the floodwaters gradually recede or decrease in volume can cause the oxidative dissolution of these As sulfides.

The speciation and geochemical investigations performed in this study suggest As in these soils may not be resistant to processes that could mobilize As in anoxic/saline conditions expected with SLR. Additionally, the area showed high levels of contamination with different other hazardous elements such as Cr and Pb. The speciation and mobility of Pb and Cr, should, therefore, be assessed in future efforts. Future work should understand how SLR impacts microbial communities and As cycling in As−contaminated soils. The interplay between salinity shifts, DOC fluctuations, and As release at different SLR scenarios must also be better understood and investigated in future studies. Additionally, exploring the efficacy of different strategies to mitigate As release due to SLR can provide valuable insights for effective management of affected areas. The heterogeneity in our micro scale analysis and some discrepancy in micro and bulk scale data underscore the spatial variability in contaminant levels and soil properties, emphasizing the need for a comprehensive understanding of the vertical distribution and characteristics of elements such as As, Fe, and S for effective environmental management and remediation efforts. The results gained here can help develop or update mitigation strategies to account for SLR−associated risks in coastal environments that currently fail to consider flooding and SLR as significant contributing factors to water pollution.

CRediT authorship contribution statement

Fatemeh Izaditame: Writing – review & editing, Writing – original draft, Visualization, Validation, Methodology, Investigation, Funding acquisition, Formal analysis, Data curation, Conceptualization. **Donald Sparks:** Writing – review & editing, Validation, Supervision, Software, Resources, Project administration, Methodology, Investigation, Funding acquisition, Conceptualization. **Ryan Tappero:** Validation, Supervision, Formal analysis, Data curation. **Xuan Yu:** Writing – review & editing, Formal analysis, Data curation. **Matthew Fischel:** Writing – review & editing, Visualization, Formal analysis. **Joshua LeMonte:** Writing – review & editing, Writing – original draft, Visualization, Methodology, Investigation, Formal analysis, Data curation, Conceptualization. **Matthew Siebecker:** Writing – review & editing, Validation, Supervision, Methodology, Formal analysis.

Declaration of Competing Interest

The authors declare the following financial interests/personal relationships which may be considered as potential competing interests: Fatemeh Izaditame reports financial support was provided by National Science Foundation. If there are other authors, they declare that they have no known competing financial interests or personal relationships that could have appeared to influence the work reported in this paper.

Data availability

Data will be made available on request.

Acknowledgement

This research is financially supported by the National Science Foundation Grant # EEC-2127509. A part of the research was under the Delaware EPSCoR's (Established Program to Stimulate Competitive Research) Project WiCCED (Water in the Changing Coastal Environment of Delaware) supported by the National Science Foundation Grant No. 1757353 and the Multistate State Hatch Project, NC1187. The authors thank the Delaware Environmental Institute (DENIN), University of Delaware Soil Chemistry group, Sheida Ghahremani for helping with Fig. S1 visualization, and John Cargill and others of the Delaware Department of Natural Resources and Environmental Control for assistance in gaining permissions for field sampling. Parts of this research used the XFM Beamline of the National Synchrotron Light Source II, a U. S. Department of Energy (DOE) Office of Science User Facility operated for the DOE Office of Science by Brookhaven National Laboratory under Contract No. DE-SC0012704.

Appendix A. Supporting information

Supplementary data associated with this article can be found in the

online version at doi:10.1016/j.jhazmat.2024.134528.

References

[1] Agency, U.S.E.P. Method 3051a: Microwave Assisted Acid Digestion of Sediments, Sludges, Soils, and Oils; Washington, D.C., USA, 1998.
[2] Andreae, M.O., 1978. Distribution and speciation of arsenic in natural waters and some marine algae. Deep Sea Res 25 (4), 391–402.
[3] Arsenic (2022, December 07). https://www.who.int/news-room/fact-sheets/detail/arsenic.
[4] Ascar, L., Ahumada, I., Richter, P., 2008. Influence of redox potential (Eh) on the availability of arsenic species in soils and soils amended with biosolid. Chemosphere 72 (10), 1548–1552.
[5] Barreto, M.S.C., Elzinga, E.J., Sparks, D.L., 2023. The adsorption of arsenate and p−arsanilic acid onto ferrihydrite and subsequent desorption by sulfate and artificial seawater: Future implications of sea level rise. Environ Pollut 323, 121302.
[6] Barreto, M.S.C., Elzinga, E.J., Kubicki, J.D., Sparks, D.L., 2024. A multi−scale assessment of the impact of salinity on the desorption of chromate from hematite: Sea level rise implications. J Hazard Mater 465, 133041.
[7] Bates, Naomi S. and John A. Callahan, 2016. Delaware Sea Level Rise Inundation Mapping Methodology. 26 pp.
[8] Bauer, M., Blodau, C., 2006. Mobilization of arsenic by dissolved organic matter from iron oxides, soils and sediments. Sci Total Environ 354 (2−3), 179–190.
[9] Bethke, C.M., Sanford, R.A., Kirk, M.F., Jin, Q., Flynn, T.M., 2011. The thermodynamic ladder in geomicrobiology. Am J Sci 311 (3), 183.
[10] Billon, G., Ouddane, B., Laureyns, J., Boughriet, A., 2001. Chemistry of metal sulfides in anoxic sediments. Phys Chem Chem Phys 3 (17), 3586–3592.
[11] Blodau, C., 2006. A review of acidity generation and consumption in acidic coal mine lakes and their watersheds. Sci Total Environ 369 (1-3), 307–332.
[12] Bowell, R.J., Alpers, C.N., Jamieson, H.E., Nordstrom, D.K., Majzlan, J., 2014. The environmental geochemistry of arsenic—an overview—. Rev Mineral Geochem 79 (1), 1–16.
[13] Burton, E.D., Johnston, S.G., Kocar, B.D., 2014. Arsenic mobility during flooding of contaminated soil: the effect of microbial sulfate reduction. Environ Sci Technol 48 (23), 13660–13667.
[14] Burton, E.D., Johnston, S.G., Kraal, P., Bush, R.T., Claff, S., 2013. Sulfate availability drives divergent evolution of arsenic speciation during microbially mediated reductive transformation of schwertmannite. Environ Sci Technol 47 (5), 2221–2229.
[15] Callahan, John A., Benjamin P. Horton, Daria L. Nikitina, Christopher K. Sommerfield, Thomas E. McKenna, and Danielle Swallow, 2017. Recommendation of Sea-Level Rise Planning Scenarios for Delaware: Technical Report, prepared for Delaware Department of Natural Resources and Environmental Control (DNREC) Delaware Coastal Programs. 116 pp.
[16] Canfield, D.E., 1989. Reactive iron in marine sediments. Geochim Et Cosmochim Acta 53 (3), 619–632.
[17] Castillo−Michel, H., Hernandez−Viezcas, J., Dokken, K.M., Marcus, M.A., Peralta−Videa, J.R., Gardea−Torresdey, J.L., 2011. Localization and speciation of arsenic in soil and desert plant Parkinsonia florida using μXRF and μXANES. Environ Sci Technol 45 (18), 7848–7854.
[18] Cooksey, S., Carter, D., & Arndt, T. (2012). Preparing for Tomorrow's High Tide Sea Level Rise Vulnerability Assessment for the State of Delaware.
[19] Crecelius, E.A., Bothner, M.H., Carpenter, R., 1975. Geochemistries of arsenic, antimony, mercury, and related elements in sediments of Puget Sound. Environ Sci Technol 9 (4), 325–333.
[20] Delaware Climate Office accessed February 20, 2024, at. ⟨https://climate.udel.edu/⟩.
[21] Delemos, J.L., Bostick, B.C., Renshaw, C.E., StÜrup, S., Feng, X., 2006. Landfill−stimulated iron reduction and arsenic release at the Coakley Superfund Site (NH). Environ Sci Technol 40 (1), 67–73.
[22] Dousova, B., Buzek, F., Herzogova, L., Machovic, V., Lhotka, M., 2015. Effect of organic matter on arsenic (V) and antimony (V) adsorption in soils. Eur J Soil Sci 66 (1), 74–82.
[23] Du Laing, G., Rinklebe, J., Vandecasteele, B., Meers, E., Tack, F.M., 2009. Trace metal behaviour in estuarine and riverine floodplain soils and sediments: a review. Sci Total Environ 407 (13), 3972–3985.
[24] Fischel, M.H.H., Clarke, C., Sparks, D.L., 2023. Synchrotron resolved microscale and bulk mineralogy in manganese-rich soils and associated pedogenic concretions. Geoderma 430, 116305.
[25] Fischel, M.H.H., Clarke, C., Sparks, D.L., 2024. Arsenic sorption and oxidation by natural manganese-oxide-enriched soils: Reaction kinetics respond to varying environmental conditions. Geoderma 441, 116715.
[26] Frommer, J., Voegelin, A., Dittmar, J., Marcus, M.A., Kretzschmar, R., 2011. Biogeochemical processes and arsenic enrichment around rice roots in paddy soil: results from micro-focused X-ray spectroscopy. Eur J Soil Sci 62 (2), 305–317.
[27] Gamble, A.V., Givens, A.K., Sparks, D.L., 2018. Arsenic speciation and availability in orchard soils historically contaminated with lead arsenate. J Environ Qual 47 (1), 121–128.
[28] Goldberg, S., Johnston, C.T., 2001. Mechanisms of arsenic adsorption on amorphous oxides evaluated using macroscopic measurements, vibrational spectroscopy, and surface complexation modeling. J Colloid Interface Sci 234 (1), 204–216.
[29] Gómez, J.A. (2021, May). Superfund EPA: Should Take Additional Actions to Manage Risks from Climate Change Effects, Statement of J. Alfredo Gómez, Director, Natural Resources and Environment, Testimony Before the Subcommittee on Environment and Climate Change, Committee on Energy and Commerce, House of Representatives. In United States. Government Accountability Office (No. GAO−21−555T). United States. Government Accountability Office.
[30] Hansel, C.M., Wielinga, B.W., Fendorf, S., 2003. Structural and compositional evolution of Cr/Fe solids after indirect chromate reduction by dissimilatory iron–reducing bacteria. Geochim Et Cosmochim Acta 67 (3), 401–412.
[31] Hingston, J.A., Collins, C.D., Murphy, R.J., Lester, J.N., 2001. Leaching of chromated copper arsenate wood preservatives: a review. Environ Pollut 111 (1), 53–66.
[32] Hopp, L., Nico, P.S., Marcus, M.A., Peiffer, S., 2008. Arsenic and chromium partitioning in a podzolic soil contaminated by chromated copper arsenate. Environ Sci Technol 42 (17), 6481–6486.
[33] Izaditame, F., Siebecker, M.G., Sparks, D.L., 2022. Sea−level−rise−induced flooding drives arsenic release from coastal sediments. J Hazard Mater 423, 127161.
[34] Khaokaew, S., Landrot, G., Chaney, R.L., Pandya, K., Sparks, D.L., 2012. Speciation and release kinetics of zinc in contaminated paddy soils. Environ Sci Technol 46 (7), 3957–3963.
[35] Kirk, M.F., Roden, E.E., Crossey, L.J., Brealey, A.J., Spilde, M.N., 2010. Experimental analysis of arsenic precipitation during microbial sulfate and iron reduction in model aquifer sediment reactors. Geochim Et Cosmochim Acta 74 (9), 2538–2555.
[36] Kocar, B.D., Fendorf, S., 2009. Thermodynamic constraints on reductive reactions influencing the biogeochemistry of arsenic in soils and sediments. Environ Sci Technol 43 (13), 4871–4877.
[37] Lafferty, B.J., Ginder−Vogel, M., Sparks, D.L., 2010. Arsenite oxidation by a poorly crystalline manganese−oxide 1. Stirred−flow experiments. Environ Sci Technol 44 (22), 8460–8466.
[38] Landrot, G., Tappero, R., Webb, S.M., Sparks, D.L., 2012. Arsenic and chromium speciation in an urban contaminated soil. Chemosphere 88 (10), 1196–1201.
[39] LeMonte, J.J., Stuckey, J.W., Sanchez, J.Z., Tappero, R., Rinklebe, J., Sparks, D.L., 2017. Sea level rise induced arsenic release from historically contaminated coastal soils. Environ Sci Technol 51 (11), 5913–5922.
[40] Loeppart, R.H., Inskeep, W.P., 1996. Iron. In: Sparks, D.L. (Ed.), In Methods of Soil Analysis. Part 3. Chemical Methods. Soil Science Society of America, Madison, WI, pp. 384–411.
[41] Lowers, H.A., Breit, G.N., Foster, A.L., Whitney, J., Yount, J., Uddin, M.N., Muneem, A.A., 2007. Arsenic incorporation into authigenic pyrite, Bengal Basin sediment, Bangladesh. Geochim Et Cosmochim Acta 71 (11), 2699–2717.
[42] Malik, A.A., Puissant, J., Buckeridge, K.M., Goodall, T., Jehmlich, N., Chowdhury, S., Griffiths, R.I., 2018. Land use driven change in soil pH affects microbial carbon cycling processes. Nat Commun 9 (1), 3591.
[43] Manceau, A., Charlet, L., 1992. X−ray absorption spectroscopic study of the sorption of Cr (III) at the oxide−water interface: I. Molecular mechanism of Cr (III) oxidation on Mn oxides. J Colloid Interface Sci 148 (2), 425–442.
[44] Mandal, B.K., Suzuki, K.T., 2002. Arsenic round the world: a review. Talanta 58 (1), 201–235.
[45] Manning, B.A., Fendorf, S.E., Bostick, B., Suarez, D.L., 2002. Arsenic (III) oxidation and arsenic (V) adsorption reactions on synthetic birnessite. Environ Sci Technol 36 (5), 976–981.
[46] Match!Phase Analysis using Powder Diffraction, Crystal Impact - Dr. H. Putz & Dr. K. Brandenburg GbR, Kreuzherrenstr. 102 53227.https://www.crystalimpact.de/match.
[47] McCauley, A., Jones, C., Jacobsen, J., 2009. Soil pH and organic matter. Nutr Manag Modul 8 (2), 1–12.
[48] Newville, M., 2013. Larch: an analysis package for XAFS and related spectroscopies (April). In: In Journal of Physics: Conference Series, Vol. 430. IOP Publishing,, 012007 (April).
[49] O'Day, P.A., Vlassopoulos, D., Root, R., Rivera, N., 2004. The influence of sulfur and iron on dissolved arsenic concentrations in the shallow subsurface under changing redox conditions. Proc Natl Acad Sci 101 (38), 13703–13708.
[50] Paper, J.M., Flynn, T.M., Boyanov, M.I., Kemner, K.M., Haller, B.R., Crank, K., Kirk, M.F., 2021. Influences of pH and substrate supply on the ratio of iron to sulfate reduction. Geobiology 19 (4), 405–420.
[51] Porell, M., Cushman, M., Fischel, J.S., Fischel, M.H., Sparks, D.L., & Grayburn, R. (2023). Scanning X-ray fluorescence spectroscopy and micro-X-ray absorption near-edge structure analysis as a guiding tool for the conservation treatment of two eighteenth-century Philadelphian portraits. X-Ray Spectrometry.
[52] Poulton, S.W., Krom, M.D., Raiswell, R., 2004. A revised scheme for the reactivity of iron (oxyhydr) oxide minerals towards dissolved sulfide. Geochim Et Cosmochim Acta 68 (18), 3703–3715.
[53] Prescher, C., Prakapenka, V.B., 2015. DIOPTAS: a program for reduction of two−dimensional X−ray diffraction data and data exploration. High Press Res 35 (3), 223–230.
[54] Quicksall, A.N., Bostick, B.C., Sampson, M.L., 2008. Linking organic matter deposition and iron mineral transformations to groundwater arsenic levels in the Mekong delta, Cambodia. Appl Geochem 23 (11), 3088–3098.
[55] Ravel, B., Newville, M., 2005. ATHENA, ARTEMIS, HEPHAESTUS: data analysis for X–ray absorption spectroscopy using IFEFFIT. J Synchrotron Radiat 12 (4), 537–541.
[56] Raven, K.P., Jain, A., Loeppert, R.H., 1998. Arsenite and arsenate adsorption on ferrihydrite: kinetics, equilibrium, and adsorption envelopes. Environ Sci Technol 32 (3), 344–349.

[57] Redman, A.D., Macalady, D.L., Ahmann, D., 2002. Natural organic matter affects arsenic speciation and sorption onto hematite. Environ Sci Technol 36 (13), 2889–2896.
[58] Rochette, E.A., Bostick, B.C., Li, G., Fendorf, S., 2000. Kinetics of arsenate reduction by dissolved sulfide. Environ Sci Technol 34 (22), 4714–4720.
[59] Saalfield, S.L., Bostick, B.C., 2009. Changes in iron, sulfur, and arsenic speciation associated with bacterial sulfate reduction in ferrihydrite-rich systems. Environ Sci Technol 43 (23), 8787–8793.
[60] Sanchez, J.Z. (2021). The impact of redox potential and salinity on arsenic cycling and mobility in iron oxide systems (Doctoral dissertation, University of Delaware).
[61] Sanders, J.G., 1980. Arsenic cycling in marine systems. Mar Environ Res 3 (4), 257–266.
[62] Sherman, D.M., Randall, S.R., 2003. Surface complexation of arsenic (V) to iron (III)(hydr) oxides: structural mechanism from ab initio molecular geometries and EXAFS spectroscopy. Geochim Et Cosmochim Acta 67 (22), 4223–4230.
[63] Smedley, P.L., Kinniburgh, D.G., 2002. A review of the source, behaviour and distribution of arsenic in natural waters. Appl Geochem 17 (5), 517–568.
[64] Smith, E.R.G., Naidu, R., & Alston, A.M. (1998). Arsenic in the soil environment. Advances in agronomy, Volume 64, Academic Press.
[65] Sparks, D.L., Page, A.L., Helmke, P.A., Loeppert, R.H. (Eds.), 2020. Methods of soil analysis, part 3: Chemical methods, Vol. 14. John Wiley & Sons.
[66] Sparks, D.L. (Ed.). (1998). Soil physical chemistry. CRC press.
[67] Sricharoenvech, P., Siebecker, M.G., Tappero, R., Landrot, G., Fischel, M.H., Sparks, D.L., 2024. Chromium speciation and mobility in contaminated coastal urban soils affected by water salinity and redox conditions. J Hazard Mater 462, 132661.
[68] Stevens, B.N., Betts, A.R., Miller, B.W., Scheckel, K.G., Anderson, R.H., Bradham, K.D., Basta, N.T., 2018. Arsenic speciation of contaminated soils/solid wastes and relative oral bioavailability in swine and mice. Soil Syst 2 (2), 27.
[69] Strawn, D., Doner, H., Zavarin, M., McHugo, S., 2002. Microscale investigation into the geochemistry of arsenic, selenium, and iron in soil developed in pyritic shale materials. Geoderma 108 (3−4), 237–257.
[70] Strawn, D.G., Sparks, D.L., 2000. Effects of soil organic matter on the kinetics and mechanisms of Pb (II) sorption and desorption in soil. Soil Sci Soc Am J 64 (1), 144–156.
[71] U.S. Environmental Protection Agency, 2007. USEPA 3051 A Microwave assisted acid digestion of sediments, sludges, soils, and oils. U.S. Environmental Protection Agency, Washington, DC, USA.
[72] U.S. geological survey (2019) Arsenic and drinking water, accessed February 20, 2024, at. https://www.usgs.gov/mission−areas/water−resources/science/arsenic−and−drinking−water.
[73] Verbeeck, M., Hiemstra, T., Thiry, Y., Smolders, E., 2017. Soil organic matter reduces the sorption of arsenate and phosphate: a soil profile study and geochemical modelling. Eur J Soil Sci 68 (5), 678–688.
[74] Vodyanitskii, Y.N., 2009. Chromium and arsenic in contaminated soils (review of publications). Eurasia Soil Sci 42 (5), 507–515.
[75] Waslenchuk, D.G., 1978. The budget and geochemistry of arsenic in a continental shelf environment. Mar Chem 7 (1), 39–52.
[76] Weil, R.R., & Brady, N.C. (2019). Elements of the nature and properties of soils. Pearson Education, Inc.
[77] Wenzel, W.W., Kirchbaumer, N., Prohaska, T., Stingeder, G., Lombi, E., Adriano, D. C., 2001. Arsenic fractionation in soils using an improved sequential extraction procedure. Anal Chim Acta 436 (2), 309–323.
[78] Weston, N.B., Dixon, R.E., Joye, S.B., 2006. Ramifications of increased salinity in tidal freshwater sediments: Geochemistry and microbial pathways of organic matter mineralization. J Geophys Res: Biogeosciences (G1), 111.
[79] Wong, V.N., Johnston, S.G., Burton, E.D., Bush, R.T., Sullivan, L.A., Slavich, P.G., 2010. Seawater causes rapid trace metal mobilisation in coastal lowland acid sulfate soils: Implications of sea level rise for water quality. Geoderma 160 (2), 252–263.
[80] Wong, V.N., Johnston, S.G., Burton, E.D., Bush, R.T., Sullivan, L.A., Slavich, P.G., 2013. Seawater−induced mobilization of trace metals from mackinawite−rich estuarine sediments. Water Res 47 (2), 821–832.
[81] Wong, V.N., Johnston, S.G., Burton, E.D., Hirst, P., Sullivan, L.A., Bush, R.T., Blackford, M., 2015. Seawater inundation of coastal floodplain sediments: short−term changes in surface water and sediment geochemistry. Chem Geol 398, 32–45.
[82] Yousefi, K., Veron, F., Buckley, M.P., 2020. Momentum flux measurements in the airflow over wind-generated surface waves. J Fluid Mech 895, A15.
[83] Yousefi, K., Veron, F., Buckley, M.P., 2021. Turbulent and wave kinetic energy budgets in the airflow over wind-generated surface waves. J Fluid Mech 920, A33.
[84] Yu, X., LeMonte, J.J., Li, J., Stuckey, J.W., Sparks, D.L., Cargill, J.G., Michael, H.A., 2022. Hydrologic control on arsenic cycling at the groundwater–surface water interface of a tidal channel. Environ Sci Technol 57 (1), 222–230.
[85] Zhang, C., Yu, Z.G., Zeng, G.M., Jiang, M., Yang, Z.Z., Cui, F., Hu, L., 2014. Effects of sediment geochemical properties on heavy metal bioavailability. Environ Int 73, 270–281.
[86] Zimmer, D., Kruse, J., Baum, C., Borca, C., Laue, M., Hause, G., Leinweber, P., 2011. Spatial distribution of arsenic and heavy metals in willow roots from a contaminated floodplain soil measured by X−ray fluorescence spectroscopy. Sci Total Environ 409 (19), 4094–4100.